Comparison of Test Signals for Aircraft Frequency Domain Identification

Peter Young* and Ronald J. Patton†
University of York, Heslington, York, England

The validity of applying frequency domain techniques to the identification of aircraft system dynamics is investigated using a simplified linear analytic model of a helicopter. A closed-loop identification of the helicopter model, with the longitudinal and lateral motions decoupled, is described. Measurement noise effects are included in the simulations. Input signals are applied to excite the system modes. Frequency response estimates are obtained by spectral analysis, and the coherence function is evaluated to indicate the likely accuracy. The transfer function coefficients are obtained by a nonlinear least-squares curve-fitting technique. With prior knowledge of the system order, the advantages of using a low peak-factor harmonic test signal for identification instead of the more usual frequency sweeps are demonstrated.

Introduction

IT is important when designing aircraft control systems to be able to analyze the sensitivity of the system to parameter variations and structural changes. Frequency domain techniques have been applied successfully by Tischler et al.[1,2] to identify open-loop aircraft dynamics and have been shown to provide considerable information concerning dynamic order and sensitivity. This paper considers the application of frequency domain techniques to the identification of helicopter dynamics. In particular, it compares two different types of test signals that can be used in frequency domain work. Although considerable work has been published on input signal design for time domain work (see, for example, Ref. 3) this is not the case in the frequency domain. A closed-loop identification in the frequency domain allows the system dynamics and handling qualities to be assessed for a range of flight conditions. Simulations of the helicopter flight using linear models of longitudinal and lateral motion with measurement noise are described. These are simplified models that do not include the higher-order noise effects due to vibration and rotor dynamics, which would be present in helicopter flight tests. The performance of the excitation waveforms in identifying the transfer functions of the models is of primary importance in this work. These signals are a sinusoidal frequency sweep and a low peak-factor, Schroeder-phased harmonic signal, as described by Schroeder[4] and Flower et al.[5] Both have approximately flat, band-limited spectral characteristics.

Each signal is applied in turn to a single control input to excite the dominant modes of the system. A frequency response estimate is obtained by spectral analysis of the time-series data. The poles and zeros of this transfer function are determined by a nonlinear least-squares curve-fitting technique and compared to the known system modes. The magnitude-squared coherence function is calculated during the spectral analysis to give a guide to the accuracy of the identification. Results are given for two transfer functions identified from simulations with measurement noise added either inside or outside the control loop. For the swept sine-wave tests, two different frequency sweep profiles were used, one linear and the other logarithmic. For sine-wave tests using a linear sweep profile, low frequency identification is generally poor and the frequency response estimates are very susceptible to the effects of noise. A logarithmic sweep-rate profile produces much better identifications due to the concentration of spectral content at lower frequencies. With Schroeder-phased signals, good frequency response estimates are achievable across the whole spectrum, and the effects of noise on the variance of the estimates is reduced. System modes can also be better identified from the Schroeder-phased frequency response estimates. The results show the advantages of using Schroeder-phased test signals to identify aircraft dynamics.

Received July 13, 1988; presented as Paper 88-4349 at the AIAA Atmospheric Flight Mechanics Conference, Minneapolis, MN, Aug. 15-17, 1988; revision received Dec. 19, 1988.

*Research Assistant, Department of Electronics.
†Senior Lecturer, Department of Electronics. Member AIAA.

Frequency Domain Methods

Input Signal Design

Each signal is applied separately to one of the system inputs and the response at one output is studied; this is single input-single output transfer function identification. For a full system identification, each input-output pair can be tested in turn and the transfer function obtained separately. The frequency sweep signal is simply a sinusoid which increases in frequency with time. Two sweep-rate profiles were used: linear, in which the frequency increases by a fixed increment with every time step, and logarithmic, in which the frequency is multiplied by a fixed scale factor at each time step. The linear sweep tends to be deficient in power spectral density at the lower frequencies but has constant spectral density at higher frequencies. The logarithmic sweep concentrates the power at the low frequency end of the spectrum at the expense of the higher frequency end and will therefore excite the low frequency system dynamics more. The Schroeder-phased signal is a multifrequency signal composed of a large number of harmonics equally spaced in frequency. Each harmonic is specified by a phase shift chosen so that when they are all added together the wave formed has a low peak-factor and fits a given power spectral density function. In this study, a signal is chosen with an approximately flat spectrum (the more harmonics, the flatter the spectrum) across the selected bandwidth. The Schroeder-phased signal has greater power spectral density than a frequency sweep of the same peak amplitude. The power spectral densities of the three signals are shown in Fig. 1. Details of how to select the phases to design a Schroeder-phased wave are given in the appendix and in Ref. 5. For a spectrum with N_s consecutive harmonics of equal power $p_i = 1/N_s$, $i = 1$ to N_s the phases should be

$$\varphi_n = (\pi/N_s)(n^2 + n) \tag{1}$$

The typical form of a Schroeder-phased signal, with period T, as used in this study is shown in Fig. 2. The amplitude of the sine wave and the mean amplitude of the Schroeder-phased

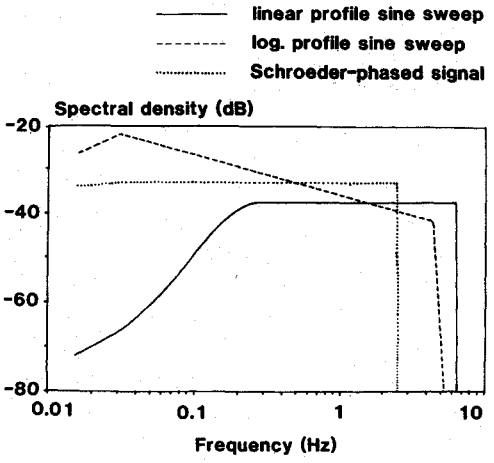

Fig. 1 Power spectral density functions of the test signals.

signal are equal. The low peak-factor of the latter means that the peak amplitude is of similar magnitude, and the two types of signal will disturb the system under test by about the same amount.

The Schroeder-phased signal used has period $T = 65.536$ s and is repeated 16 times. It is composed of 160 harmonics in the frequency range 0.015–2.5 Hz. Each frequency sweep range is one cycle long with a range of 0.015 to 4.0 Hz (linear) or to 2.5 Hz (logarithmic), but the total time for which the signal is applied is the same as for the harmonic signal.

Spectral Analysis

Standard spectral techniques are applied to the input and output data sequences to obtain the auto- and cross-power spectral density functions, the frequency response estimate, and the coherence function. A direct method of spectral estimation using the overlapped fast Fourier transform (FFT) processing described by Carter and Ferrie[6] is used. Several steps are required for the estimation. First, the data are divided into K segments, each of M points. Each corresponding time segment pair (input and output) is selected and processed in turn to obtain a spectral density estimate. Then the input and output data for a particular segment are multiplied by a cosine weighting function to reduce the side-lobe leakage. As some of the data are lost when weighting is applied, a segment overlap of 62.5% in the FFT processing is employed to compensate. Carter et al.[7] have shown that this value maximizes the improvement in the spectral estimate possible from overlapping. As the identification is not performed in real time, computation time is not critical; therefore the full 62.5% overlap is used. The discrete Fourier transform of the weighted data input and output segments is taken using a radix-2 FFT algorithm. Averaging the squared modulus of the Fourier coefficients obtained (at a given frequency) over all the segments gives an estimate of the spectral density function. This amounts to averaging a number of spectral estimates (each found from a data segment) over the whole data series.

The auto- and cross-power spectral estimates are determined as

$$\hat{G}_{xx}(k) = \frac{1}{Kf_sM} \sum_{n=1}^{K} |X_n(k)|^2 \tag{2}$$

$$\hat{G}_{yy}(k) = \frac{1}{Kf_sM} \sum_{n=1}^{K} |Y_n(k)|^2 \tag{3}$$

$$\hat{G}_{xy}(k) = \frac{1}{Kf_sM} \sum_{n=1}^{K} |X_n^*(k)Y_n(k)|^2 \tag{4}$$

where f_s is the sample frequency, k the discrete frequency variable, G_{xx} and G_{yy} the input and output autospectral densities, and G_{xy} the cross-spectral density. The transfer function is defined as

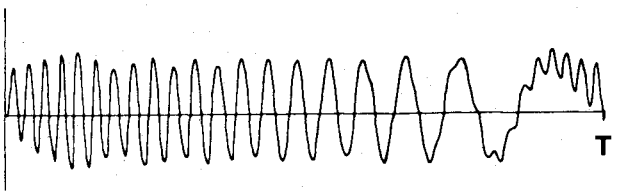

Fig. 2 The Schroeder-phased signal.

$$\hat{H}(k) = [\hat{G}_{xy}(k)]/[\hat{G}_{xx}(k)] \tag{5}$$

This is strictly true only when the measurement noise is uncorrelated with the input and the output but is suitable as an approximation for examples in this paper where this is not the case. The frequency response estimate is found using Eq. (5). The variance of spectral estimates is reduced by the averaging of estimates from successive data frames. An expression can be derived[8] for the variance of frequency response estimates in terms of the coherence function as explained in the next section. This variance is inversely proportional to the number of data frames K. When choosing suitable frame lengths for a fixed total data length, a balance must be found between this variance and the bias introduced by shorter frame lengths.

The precision and resolution of the spectral estimate depends on the choice of N, the number of data samples, and M, the segment size, respectively. The analysis of Priestley[9] can be applied here to evaluate suitable minimum values for M and N and the ratio between them. The minimum value for M depends on the required degree of resolution, that is, the ability to distinguish fine detail in the spectral density functions. It also depends on the data window used, in this case the Tukey-Hanning window (also described by Priestley). For a given value of M, there is a certain minimum value of N, which depends on the precision required in the spectral estimates. The frequency range of interest is 0.015–4.0 Hz. So the theoretical minimum sample rate (f_s) is 8 Hz. An acceptable sample rate needs to be much greater than this and f_s was chosen to be 31.25 Hz. A minimum resolvable frequency of 0.015 Hz was desired and using Priestley's equations we obtain $M = 1307$. For a proportional error not exceeding 25% at the 90% confidence level, this would give $N = 61103$. However, with 62.5% segment overlap, fewer points are required as each is used more than once. In fact, the number of points needed is approximately $N' = 3N/8$ giving $N' = 22914$ for this example. To make use of the radix-2 FFT algorithm M was selected as 2048, and the corresponding N' was 32,768. A greater value of M would give better resolution as the window bandwidth is decreased and, in general, a larger value of N would allow M to be increased without loss of precision. About 17 min of flight test data would be required to satisfy these criteria in practice. This seems a long time but can be justified as multiple runs can be concatenated.

The Coherence Function

The magnitude-squared coherence function gives an indication of how good the first harmonic is as a model of the input-output dynamics. It is a measure of the linear dependence of the output on the input defined in spectral terms:

$$\gamma_{xy}^2(k) = \frac{|G_{xy}(k)|^2}{|G_{xx}(k)||G_{yy}(k)|} \leq 1 \tag{6}$$

Consider the closed-loop system of Fig. 3a where noise is added at the output but the uncontaminated output $z(t)$ is fed back to close the loop. Coherence can then be expressed in

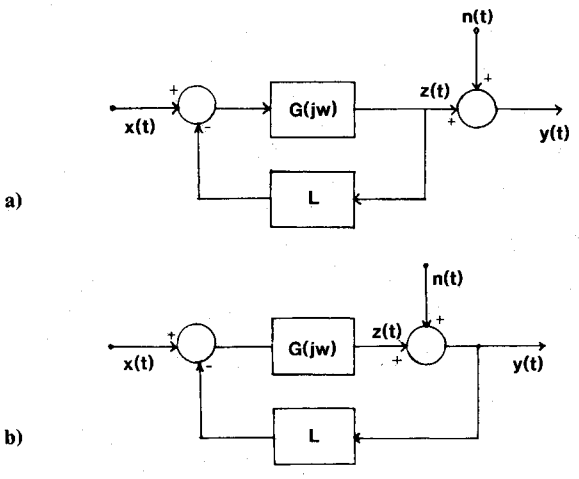

Fig. 3 System with measurement noise: a) outside control loop; b) inside control loop.

terms of the frequency domain representation of the system signal-to-noise ratio:

$$\gamma_{xy}^2(k) = \frac{1}{1 + G_{nn}(k)/G_{zz}(k)} \tag{7}$$

G_{zz} is the autospectrum of the uncontaminated output and G_{nn} is the input autospectrum of the noise. A totally noise-free linear system would yield $\gamma_{xy}^2 = 1$. A coherence of less than unity may be due to three causes: system nonlinearity, input and output noise, and secondary inputs (e.g., external disturbances). When the system is noisy or nonlinear, the coherence function indicates the accuracy of an identification as a function of frequency. The closer it is to unity, the more accurate the identification is likely to be at a particular frequency. This is reflected in the fact that the variance of a frequency response estimate obtained during spectral analysis is inversely proportional to the coherence function:

$$\frac{\mathrm{Var}\{|H(j\omega)|\}}{|H(j\omega)|} = \mathrm{Var}\{\arg H(j\omega)\} = \frac{1}{2K}\left(\frac{1}{\gamma_{xy}^2} - 1\right) \tag{8}$$

When the noisy output $y(t)$ is fed back to close the loop (see Fig. 3b), as would be the case where the sensor outputs from a system are used for control, Eq. (7) is not applicable. In this case, the output $z(t)$ and the noise are correlated due to the feedback action. The cross-spectral estimate derived in Eq. (4) and used to evaluate the frequency response estimate and the coherence in Eqs. (5) and (6) assumes the output to be uncorrelated with the noise. However, Eqs. (5) and (6) are suitable approximations for use in this study.

Least-Squares Curve Fitting

A transfer function is obtained by fitting the frequency response estimate algebraically as a ratio of two frequency-dependent polynomials:

$$\frac{P(s)}{Q(s)} = \frac{p_0 + p_1 s + p_2 s^2 + \ldots + p_m s^m}{q_0 + q_1 s + q_2 s^2 + \ldots + q_n s^n} \tag{9}$$

where $s = j\omega$, the complex frequency variable. Least-squares techniques are employed to minimize a given error criterion and to derive the set of transfer function coefficients that gives the best algebraic fit to the complex curve. The following least-squares criterion is an obvious choice, but as it is nonlinear in the parameters $q_0, q_1, \ldots, q_n$ the minimization is quite complex

$$E = \sum_{k=1}^{N} \left| \frac{P(j\omega_k)}{Q(j\omega_k)} - F(j\omega_k) \right|^2 \tag{10}$$

$F(j\omega)$ is the actual frequency response data, and N is the number of frequency response samples. A number of linear approaches have been developed to simplify the approach to the solution, and a comparison of these has been made by Whitfield.[10] The method of Sanathanan and Koerner[11] has been used with some success by the authors.[12] However, it has been shown that, when convergent, the solution from this method does not tend asymptotically to the solution of the nonlinear least-squares criterion.[13] In particular, if the frequency response data are noisy, the accuracy of the transfer function evaluated deteriorates with the noise level. This problem of biased estimation is typical of linear least-squares methods.

The Levenberg-Marquardt form of the Gauss-Newton, nonlinear, least-squares method[14] is applied to improve the identification of the transfer function coefficients for noisy systems. This is an iterative search procedure that interpolates between a Gauss-Newton method, which converges rapidly when the initial parameter estimates are good and a steepest descent method which converges with poor starting estimates but can take rather a long time. By changing gradually between the methods (depending on how close the parameters are to the minimum at each iteration), the dual advantage of both methods can be gained. A description of all these nonlinear least-squares methods is given by Bevington.[15] The derivation of the nonlinear least-squares method and the procedure are described fully in the paper by Marquardt.[14] To obtain suitable starting values, a linear least-squares optimization is carried out first using the method of Sanathanan and Koerner, and the evaluated transfer function coefficients are then used as the initial parameters in the nonlinear optimization. Reasonably good starting values help to minimize computation time and reduce the likelihood of the optimization converging to a local minimum solution rather than the global one. In the authors' experience, this method always converges, finding the global minimum solution, although convergence is not rigorously proven.

The Helicopter Model

The linear mathematical model used in this study is based on that of Hendricks[16] and is derived from a nonlinear model of a helicopter developed using the standard aerodynamic equations given by Bramwell[17] with minor approximations. Longitudinal and lateral motions are assumed to be decoupled. A four-state longitudinal model and a five-state lateral model are considered separately.

Longitudinal Motion

The control inputs and state variables for the longitudinal degrees of freedom are

$$u(t) = (b_1, \theta_0)^T, \qquad x(t) = (u, w, \theta, q)^T$$

where b_1 is longitudinal cyclic pitch and θ_0 is collective pitch. The states are horizontal velocity u, vertical velocity w, pitch angle θ, and pitch rate q.

For the flight condition with a tip-speed ratio μ of 0.1 and zero angle of attack, the open-loop stability and control derivative matrices (A_1 and B_1) are known:

$$A_1 = \begin{bmatrix} -0.10 & 0.01 & -9.81 & 0.00 \\ -3.00 & -1.27 & 0.00 & 7.12 \\ 0.00 & 0.00 & 0.00 & 1.00 \\ 0.41 & -0.37 & 0.00 & -0.70 \end{bmatrix}$$

$$B_1 = \begin{bmatrix} 9.74 & 0.03 \\ 9.03 & -64.75 \\ 0.00 & 0.00 \\ -32.15 & -0.11 \end{bmatrix}$$

A feedback controller (L_1) has been chosen:

$$L_1 = \begin{bmatrix} 1.7\times10^{-3} & 7.4\times10^{-3} & -0.36 & -0.22 \\ 6.1\times10^{-3} & -3.0\times10^{-3} & 1.1\times10^{-3} & 1.5\times10^{-2} \end{bmatrix}$$

The system closed-loop matrix is

$$D_1 = A_1 - B_1 L_1 \tag{11}$$

The corresponding resolvent matrix $\Phi_1(s)$ is

$$\Phi_1(s) = (sI - D_1)^{-1} \tag{12}$$

Lateral Motion

In the lateral case, the control inputs and states are

$$u(t) = (a_1, \theta_t)^T, \qquad x(t) = (v,\varphi,p,\psi,r)^T$$

where a_1 is lateral cyclic pitch and θ_t is tail rotor pitch. The states are sideslip velocity v, bank angle φ, roll rate p, heading angle ψ, and yaw rate r.

Under the same flight conditions as applied for the longitudinal model, the A and B matrices are

$$A_2 = \begin{bmatrix} -0.24 & 9.81 & 0.00 & 0.00 & -7.54 \\ 0.00 & 0.00 & 1.00 & 0.00 & 0.00 \\ -0.40 & 0.00 & -1.76 & 0.00 & 0.00 \\ 0.00 & 0.00 & 0.00 & 0.00 & 1.00 \\ 1.12 & 0.00 & 0.00 & 0.00 & -1.08 \end{bmatrix}$$

$$B_2 = \begin{bmatrix} -9.81 & 2.86 \\ 0.00 & 0.00 \\ -111.50 & 0.00 \\ 0.00 & 0.00 \\ 0.00 & 39.04 \end{bmatrix}$$

An eigenstructure assignment technique was used to design the closed-loop lateral motion regulator. The same flight conditions apply as in the longitudinal case. The design was achieved using a package developed by Mudge and Patton.[18] The aim of this assignment was to decouple the Dutch-roll mode from roll subsidence giving improved handling qualities and damping. With five states and two controls, two elements in each vector can be assigned along with all the eigenvalues. This is the case as the full state-feedback system $\{A_2, B_2\}$ is controllable, and the maximum assignment freedom can be fully utilized. The eigenstructure is assigned to the closed-loop matrix D_2 as follows (the order of modes is Dutch roll, roll subsidence, spiral, heading integration):

Eigenvalues:

$$-1.5 \pm j1.5 \quad -4 \quad -0.05 \quad -10$$

Eigenvectors:

$$\begin{array}{c} v: \\ \varphi: \\ p: \\ \psi: \\ r: \end{array} \begin{bmatrix} 1 \\ 0 \\ 0 \\ x \\ x \end{bmatrix} \begin{bmatrix} x \\ 0 \\ 0 \\ x \\ 1 \end{bmatrix} \begin{bmatrix} 0 \\ x \\ 1 \\ x \\ 0 \end{bmatrix} \begin{bmatrix} 0 \\ 1 \\ x \\ x \\ x \end{bmatrix} \begin{bmatrix} 1 \\ 0 \\ 1 \\ 0 \\ 1 \end{bmatrix}$$

x denotes an element whose sign and magnitude is insignificant. The lateral controller gains are

$$L_2 = \begin{bmatrix} 2.1\times10^{-3} & -0.36 & -0.11 & -1.3\times10^{-2} & -7.5\times10^{-4} \\ 2.2\times10^{-2} & 1.36 & 0.33 & 5.5\times10^{-2} & 4.6\times10^{-2} \end{bmatrix}$$

The closed-loop resolvent matrix is found as before from Eqs. (11) and (12).

Noise in the Model

The effect that measurement noise has on the system and the identification depends on whether or not it is correlated with the input and output. It also depends on whether we are identifying the open-loop dynamics from a closed-loop system or the closed-loop dynamics themselves as is the case here.

When measurement noise is added at the output of the system, and outside of the control loop as shown in Fig. 3a, it does not affect the aircraft response, but it does contaminate data. It is uncorrelated with the input and output and causes random errors in the frequency response with a corresponding decrease in the coherence function. The net effect is to increase the variance of the spectral estimates. A more realistic case is where the output with measurement noise $[y(t)]$, from sensors in the real aircraft system, is fed back to close the loop as in Fig. 3b. The noise does not affect the aircraft response as it is correlated with the output $[z(t)]$ through the feedback loop. The net result is bias in the spectral estimates. When identifying the open-loop dynamics from a closed-loop identification, the analytical treatment of bias error given by Tischler[2] is applicable. However, in this work, the closed-loop dynamics themselves are being identified, and the bias can actually be measured. It is straightforward to show that the closed-loop frequency response is the sum of the true closed-loop frequency response and a bias error term

$$\frac{G_{xy}(k)}{G_{xx}(k)} = \frac{G_{xz}(k)}{G_{xx}(k)} + \frac{G_{ny}(k)}{G_{nn}(k)} \tag{13}$$

Referring to Fig. 3b, in this equation, G_{xz} is the cross-spectral density of the noise-free estimate, G_{ny} is the cross-spectral density between the noise and the measured output and G_{nn} is the auto-spectral density of the noise. The bias error term G_{ny}/G_{nn} is the transfer function $n(t)/y(t) = 1/[1 + G(j\omega)L_2]$ when $x(t)$ is zero. When identifying the main diagonal elements of the transfer function matrix, $G(j\omega)L_2$ will be large, and therefore the bias error will be small. Only when identifying cross-coupling terms is the bias likely to be significant. The coherence function as derived in Eqs. (2-4) and Eq. (6) is considered for the noise in the loop situation but is only an approximation for the reasons outlined previously. In the simulations Gaussian white measurement noise is added at the output, and this is assumed to be realistic.

Identification of the Helicopter Dynamics

Longitudinal Results: Identification of the Transfer Function q/Θ_0

The transfer function relating pitch rate q to collective pitch Θ_0 has been computed using the Leverrier algorithm applied to the closed-loop matrix, which is a nonminimum phase system:

$$H(s) = \frac{-0.11s(s + 0.35)(s - 73.54)}{[(s + 0.58)^2 + 0.14](s + 2.68)(s + 5.44)} \tag{14}$$

This transfer function is a low-amplitude cross-coupling term that in practice may be difficult to identify. However, the standard deviation of the measurement noise added in the simulations is $\hat{q}_n = 5$ mrad s^{-1}. This has been chosen to be considerably larger than the 2 mrad s^{-1} quoted by Souza et

al.[19] for a fixed-wing aircraft and the 0.45 mrad s^{-1} quoted by Gelb[20] for a guided missile. As we are considering measurement noise only, and higher-order vibration effects are likely to be outside the frequency range of interest or else filtered by vibration isolation of the instrument, this value of $\hat{q}_n$ was felt to be realistic.

Example 1

The frequency response estimates from simulations with measurement noise of standard deviation $\hat{q}_n = 5$ mrad s^{-1} added to the output outside of the control loop (see Fig. 3a) were obtained for two input signals. These estimates are shown in Fig. 4 where three curves are plotted: the actual transfer function, the estimate obtained with a linear profile swept frequency input, and the estimate obtained with a Schroeder-phased input composed of 160 harmonics. The frequency response estimate for the Schroeder-phased identification is clearly much closer to the known transfer function than the sine-wave identification. This is particularly true at the low frequency end of the spectrum where the sine wave produces very poor results. The noise introduces variance into the estimates, especially noticable at the higher frequencies, and the sine wave estimate is more susceptible to this. Although the two input signals are of the same amplitude, the power spectral density is greater at all frequencies for the Schroeder-phased signal. This increased input power and the correspondingly better signal-to-noise ratio account for the better identification obtained when using the harmonic signal rather than a linear profile swept sine wave. The coherence functions for the two noisy simulations are shown in Fig. 5. The coherence for the Schroeder-phased estimate is close to unity over a much greater frequency range and indicates that we can rely on the identification obtained across a wider spectrum. It seems reasonable to assume that we can rely on the transfer function estimate over the frequency range for which, say, the coherence function is greater than 0.8. This is about one and a half decades of frequency for the Schroeder-phased case compared with less than one decade for the sine-wave case.

The modes identified from the two frequency response estimates are compared with the actual known modes [see Eq. (13)] in Table 1. As expected from the frequency response estimates and coherence functions, the modes are obtained more accurately from the Schroeder-phased test than from the sine-wave test. In the former case, the complex pole pair is identified well, and the real poles at -2.68 and -5.44 are also identified as a complex pair just off the real axis between these two values. The two low-frequency zeros are located quite precisely. The right-hand half-plane zero is too large to have any influence in the frequency range of interest and so a two zero model is considered. From the sine-wave estimate, the

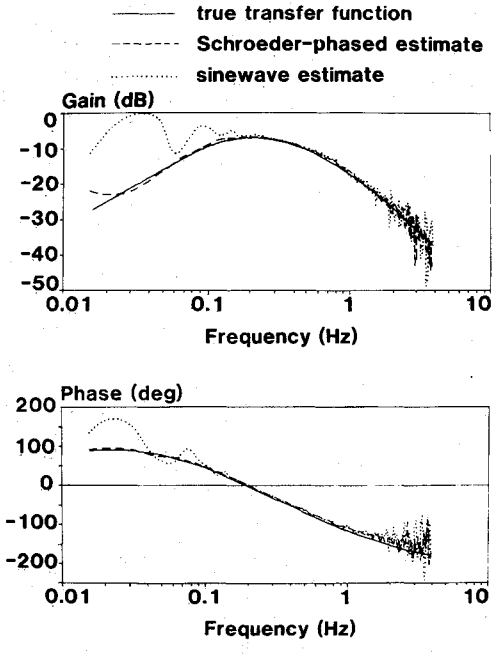

Fig. 4 Frequency response estimates of longitudinal transfer function q/Θ_0 with noise outside loop.

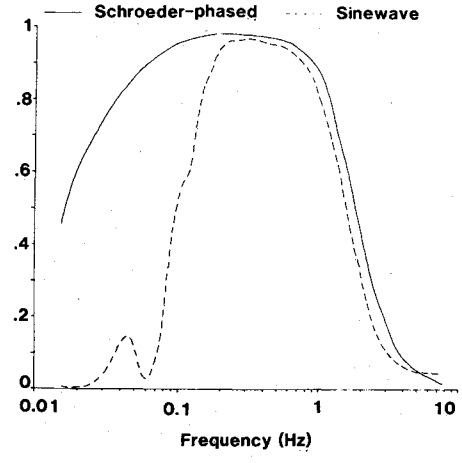

Fig. 5 Coherence function for identification of q/Θ_0 with noise outside loop.

Table 1 True and identified modes for longitudinal transfer function q/Θ_0

		Schroeder-phased identifications			Sine-wave identifications		
	True modes	Noise-free	Noise out of loop	Noise in loop	Noise-free	Noise out of loop	Noise in loop
Zeros:	-0.35	-0.54	-0.49	-0.92	0.39	0.43	0.44
	0.00	0.01	0.00	0.01	20.25	3.22	3.38
	73.54						
Poles:	-5.44	-5.36	$-3.91 \pm j0.80$	$-3.39 \pm j2.63$	-5.11	-4.28	$-3.14 \pm j1.53$
	-2.68	-2.81			-2.87	-3.30	
	$-0.58 \pm j0.37$	$-0.65 \pm j0.45$	$-0.57 \pm j0.47$	$-0.52 \pm j0.69$	-0.45	-0.42	-0.44
					22.25	3.46	4.12
Gain:	-0.11	-0.02	-0.18	-0.09	-0.05	-0.07	-0.21
χ_ν^2:	——	4×10^{-6}	6×10^{-5}	5×10^{-4}	3×10^{-4}	2×10^{-3}	2×10^{-3}

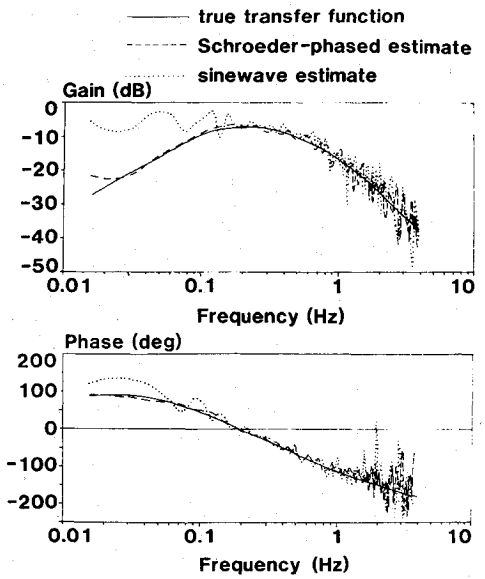

Fig. 6 Frequency response estimates of longitudinal transfer function q/Θ_0 with noise inside loop.

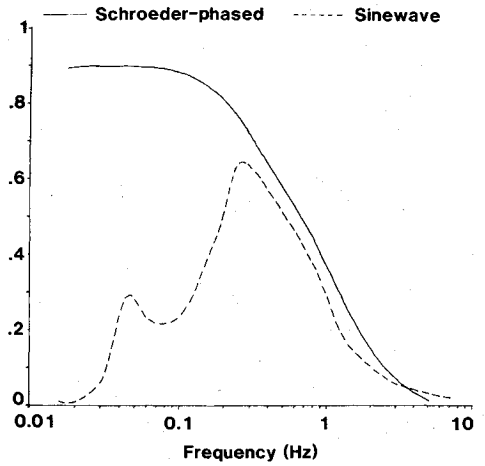

Fig. 7 Coherence function for identification of q/Θ_0 with noise inside loop.

two fast poles are identified as real but are not found very accurately. None of the zeros are identified correctly, but this is also true for the noise-free sine-wave test. Also with the sine-wave estimate, a cancelling pole-zero pair is found in both the noise-free and noisy cases (its value is not important). The curve fit is unable to identify the correct number of modes and suggests a third order fit would be more appropriate. This is the case for both noise-free and noisy identifications. Clearly, the Schroeder-phased result is much better than the sine-wave one. It is possible to band-limit the curve fit to both estimates by applying the coherence criterion and only using frequency response data at frequencies where the coherence exceeds 0.8. This produces a marginal improvement in the identified modes.

The identified gain and a measure of goodness-of-fit for the curve are also given in the table for each identification. The goodness-of-fit criterion is

$$\chi_\nu^2 = \chi^2/\nu \tag{15}$$

where the number of degrees of freedom ν is the number of data points in the frequency response estimate minus the number of parameters (the transfer function coefficients). The goodness-of-fit gives a quantitative assessment of the accuracy with which the fitted curve represents the frequency response estimate. In general, if it is greater than unity, the fitting function is not appropriate for describing the data. Where the system order is known, this implies that the poor fit is due to working on a poor frequency response estimate. It can be seen from Table 1 that in this example a closer fit is obtained for the Schroeder-phased estimate.

Example 2

The same transfer function was identified using the same test signals as before but the output with added measurement noise of standard deviation $\hat{q}_n = 0.005$ is fed back to close the control loop (see Fig. 3b). Figure 6 shows the frequency response estimates compared with the actual transfer function, and Fig. 7 shows approximate coherence functions. As in the previous example, the Schroeder-phased identification is good over a much greater frequency range than the sine-wave identification. The frequency response estimate is close to the actual transfer function, and the modes are identified more accurately. In this example, the coherence function is useful only as a *guide* to the frequency range over which the estimate is acceptable. It emphasizes the considerably better low-frequency performance of the Schroeder-phased identification. The modes are given in Table 1. As before curve-fitting to the Schroeder-phased estimate gives a good identification of the poles; although they are not as accurate as in the first example. The complex pair of poles that approximates the two fast real poles are further from the real axis and not even as close to it as the equivalent complex pair found from the sine-wave estimate. A single pole found at -0.44 from the sine-wave estimate does not compare well with the quite precise complex pair obtained from the Schroeder-phased estimate. Identification of the two dominant zeros is again quite good for the Schroeder-phased case but not in the case of the sine wave. As before, the results for the sine-wave test wrongly indicate that a third-order fit would be better.

The normalized bias error was measured in these identifications as this can be significant when identifying low-amplitude, cross-coupling terms as explained in the previous section. The bias is frequency dependent and varied from less than 0.5% at low frequencies to a maximum of around 5% at high frequencies, regardless of test signal type, which is an acceptably small level of error.

Lateral Results: Identification of the Transfer Function p/a_1

The transfer relating roll rate p to lateral cyclic pitch a_1 is

$$H(s) = \frac{-111.48s[(s+1.50)^2 + 1.50^2](s+0.14)}{[(s+1.50)^2 + 1.50^2](s+0.05)(s+4.00)(s+10.00)} \tag{16}$$

The Dutch-roll mode is not present in this transfer function as it has been decoupled from the roll subsidence mode through the eigenstructure design. This is evident from the complex pole-zero cancellation.

This transfer function is a much more significant term than the previous example. As it has a much larger gain, a much greater measurement noise, representing a worst case situation, is added to the output so that the effects of noise can be seen. The standard deviation of the measurement noise in this case is $\hat{p}_n = 0.1$.

Example 3

The frequency response estimates were obtained by identifying a simulation with measurement noise of standard deviation $\hat{p}_n = 0.1$ added to the output and with the noisy output being fed back to close the control loop. This time the sine-wave signal has a logarithmic sweep-rate profile. Otherwise the tests were carried out as before. The frequency response

estimates are shown in Fig. 8. They show that both identifications are quite good. The sine-wave estimate is marginally closer to the true estimate at low frequencies, but the Schroeder-phased estimate is less subject to noise with a smaller variance at high frequencies. The coherence functions associated with these identifications are shown in Fig. 9, and they confirm the relative accuracy of the two estimates. The sine-wave estimate has the greater coherence at low frequencies where its power spectral density is greater; the reverse is true at higher frequencies. The modes found by applying the Levenberg-Marquardt method are given in Table 2. A third-order model with two zeros is appropriate. The two fast poles at -4 and -10 are identified quite accurately from both estimates. As the noise introduces much less variance than it did in the longitudinal examples and the coherence function is close to unity across the frequency range where these poles lie, it is not surprising that the identification of these poles is good. In the real transfer function, there are two real zeros and one pole close together near the origin. Only one zero is identified in this region, as an effective cancellation of a pole-zero pair occurs, and so the system appears to be second order with one zero; this result is the one given in the table. This applies to the noise-free case as well. This zero is -0.11 for the Schroeder-phased estimate and -0.09 for the sine-wave estimate. In both cases, it lies between the two true zeros. On balance, the modal identification is a little better for the harmonic signal than for the sine-wave signal.

The normalized bias error was measured in these identifications and was found never to exceed about 2%, which is a fairly insignificant error.

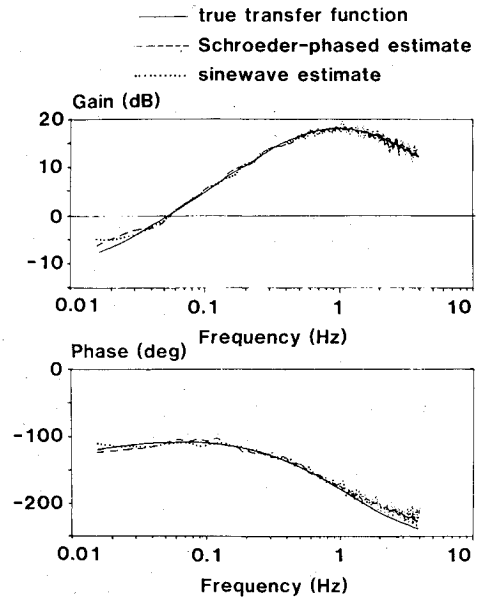

Fig. 8 Frequency response estimates of lateral transfer function p/a_1 with noise inside loop.

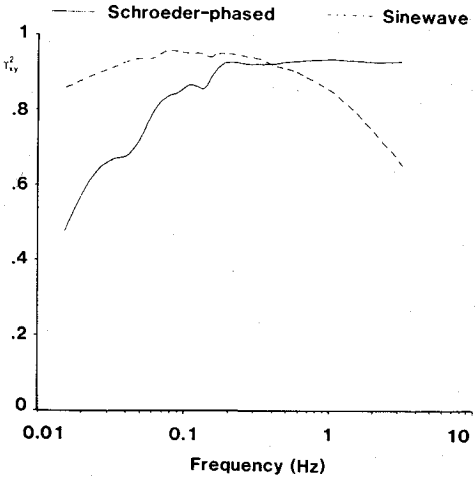

Fig. 9 Coherence function for identification of p/a_1 with noise inside loop.

Example 4

The lateral transfer function p/a_1 was again identified, but this time the noise ($\hat{p}_n = 0.1$) is added outside the control loop. The frequency response estimates and corresponding coherence functions are very similar to those in the previous example. Both identifications are acceptable over the full frequency range. The identified system modes are given in Table 2. As before the poles at -4 and -10 are quite precisely located for both identifications, although the Schroeder-phased values are closer to the true ones. The same pole-zero cancellation occurs resulting in only one zero being found near the origin. The Schroeder-phased identification determines the modes, though not the gain, more accurately than the logarithmic sweep-rate profile.

Conclusions

The frequency domain techniques that have been described are capable of accurately identifying noisy linear systems if suitable test signals are used. The longitudinal dynamic examples show that using a Schroeder-phased test signal produces a better identification of the vehicle dynamics for a given signal amplitude than a sinusoidal frequency sweep with a linear, sweep-rate profile. The frequency response estimates and the transfer functions obtained are more accurate. This is because the power spectral density of the Schroeder-phased signal is greater across the whole spectrum. The low peak-factor of the Schroeder-phased signal allows large system perturbations to be avoided and makes identification possible with a lower amplitude input. The improvement gained from using it is particularly significant at low frequencies where the linear-swept frequency sine wave is deficient in spectral content. The lateral examples show that giving the sinusoidal signal a logarithmic sweep-rate profile makes it a considerably better test

Table 2 True and identified modes for lateral transfer function p/a_1

		Schroeder-phased identifications			Sine-wave identifications		
	True modes	Noise-free	Noise out of loop	Noise in loop	Noise-free	Noise out of loop	Noise in loop
Zeros:	−0.14	−0.09	−0.11	−0.15	−0.09	−0.09	−0.08
	0.00						
Poles:	−10.00	−9.82	−9.51	−9.50	−9.75	−9.42	−9.37
	−4.00	−4.04	−4.13	−4.32	−4.07	−4.17	−4.21
	−0.05						
Gain:	−111.48	−120.23	−104.65	−110.75	−119.81	−110.70	−111.22
χ_p^2:	—	7×10^{-2}	0.29	0.23	7×10^{-2}	0.31	0.12

signal for identification. There is not much difference in the accuracy of the frequency response estimates obtainable from this sweep signal and the Schroeder-phased signal, although the effect of measurement noise is less with the latter giving a smaller variance at high frequencies. The Schroeder-phased signal also allows more precise determination of the modes. However, how good an identification is at a particular frequency is directly related to the power spectral density of the input signal at that frequency. As a result, the relative accuracy of transfer function determination using these test signals will depend to some extent on the distribution of the poles and zeros.

Good frequency response estimates have been obtained from systems where measurement noise is present. Where this noise is outside the aircraft control loop, the accuracy of an identification is directly related to the closeness of the coherence function to unity. By extension of the coherence concept, these techniques are also applicable to identifying systems with some nonlinearity. Noise occurring within the control loop causes bias errors in the frequency response estimates, but these were found to be quite small (<5%) even when identifying cross-coupling terms.

The performance of the curve-fitting procedure in finding the poles and zeros from a noisy frequency estimate is improved by using a nonlinear least-squares method rather than a linear one. The Levenberg-Marquardt method has been used with starting parameters derived from a linear, least-squares fit, and this combination has been shown to produce satisfactory results. Poles and zeros which lie close together at low frequencies are not identified by curve fitting to either Schroeder-phased or sine-wave estimates, suggesting that even lower frequency excitation may be needed to fully identify some transfer functions.

Appendix: Design of Schroeder-Phased Test Signals

The relative peak-factor of a periodic signal can be defined as

$$\text{Relative peak-factor} = \frac{|V_{\max} - V_{\min}|}{2\sqrt{2}V_{\text{rms}}} \tag{A1}$$

In identification, a test signal with a low peak-factor will avoid large perturbations in the system which is obviously desirable. It is possible to select the phase angles of a number of harmonics so that when they are summed together they produce a low peak-factor wave that fits a given power spectral density. Such a wave is a Schroeder-phased wave and is derived as follows.

The Fourier series of a wide-band signal of period T is

$$V(t) = \sum_{k=1}^{N_s} \sqrt{2}p_k \cos(2\pi kt)/T + \Theta_k) \tag{A2}$$

Θ_k is the phase angle, p_k the relative power of the kth harmonic, and N_s the number of harmonics. By definition

$$\sum_{k=1}^{N_s} p_k = 1 \tag{A3}$$

To design the wave from a particular set of values of p_k, the values of Θ_k are chosen to minimize $V_{\max} - V_{\min}$. Consider a phase-modulated signal:

$$s(t) = \cos[\Phi(t)] \tag{A4}$$

$$\Phi(t) = \int_0^t \dot{\Phi}(t)\, dt \text{ with } \dot{\Phi}(t) = 2\pi k/T \tag{A5}$$

in an interval between t_{k-1} and t_k with

$$t_k = T \sum_{j=0}^{k} p_j \qquad \text{(i.e., } t_0 = 0) \tag{A6}$$

During a time interval from t_0 to t_1, the instantaneous phase of $s(t)$ is

$$\Phi(t) = \varphi_0 + 2\pi t/T \tag{A7}$$

φ_0, the phase at $t = 0$ can be set to zero without loss of generality. Therefore

$$\Phi(t_1) = 2\pi t_1/T = 2\pi p_1 = \varphi_1 \tag{A8}$$

During the time interval from t_1 to t_2

$$\Phi(t) = \varphi_1 + \frac{2\pi}{T}\int_{t_1}^{t_2} 2\, dt = 4\pi(t - t_1)/T \tag{A9}$$

$$\Phi(t_2) = 2\pi(p_1 + 2p_2) = \varphi_2 \tag{A10}$$

In general

$$\varphi_n = 2\pi \sum_{i=1}^{n} ip_i, \qquad i = 1,\ldots,N_s \tag{A11}$$

Equation (A11) is used to adjust Θ_k in Eq. (A2). With N_s harmonics of equal power p_i

$$\varphi_n = \frac{2\pi}{N_s}\sum_{i=1}^{n} i = \frac{\pi}{N_s}(n^2 + n) \tag{A12}$$

The term $\pi n/N_s$ is a linear-phase delay. A Schroeder-phased signal with a flat spectrum can be designed, using Eqs. (A5) and (A12), specifying the frequency range and the number of harmonics. In the more general case, Eqs. (A5) and (A11) can be used to design a low peak-factor wave with any power spectral density function.

Acknowledgment

The authors would like to acknowledge the support of the United Kingdom Science and Engineering Research Council and the Royal Aircraft Establishment in funding this work under Grant XG/10732.

References

[1]Tischler, M. B., Leung, J. G. M., and Dugan, D. C., "Identification and Verification of Frequency-Domain Models of XV-15 Tilt-Rotor Aircraft Dynamics in Cruising Flight," *Journal of Guidance, Control, and Dynamics*, Vol. 9, No. 5, 1986, pp. 446–453.

[2]Tischler, M. B., "Frequency-Response Identification of XV-15 Tilt-Rotor Aircraft Dynamics," NASA TM89428, May 1987.

[3]Plaetschke, E., and Schulz, G., "Practical Input Signal Design," AGARD Lecture Series LS-104, 1979, pp. 3.1–3.19.

[4]Schroeder, M. R., "Synthesis of Low Peak-Factor Signals and Binary Sequences of Low Auto-correlation," *IEEE Transactions on Information Theory*, Vol. 16, Jan. 1970, pp. 85–89.

[5]Flower, J. O., Knott, G. F., and Forge, S. C., "Application of Schroeder-Phased Harmonic Signals to Practical Identification," *Measurement and Control*, Vol. 11, Feb. 1978, pp. 69–73.

[6]Carter, C. G., and Ferrie, J. F., "A Coherence and Cross-Spectral Estimation Program," *Programs for Digital Signal Processing*, Inst. of Electrical and Electronics Engineers, New York, 1979.

[7]Carter, C. G., Knapp, C. H., and Nuttall, A. H., "Estimation of the Magnitude-Squared Coherence Function via Overlapped Fast Fourier Transform Processing," *IEEE Transactions on Audio and Electroacoustics*, Vol. 21, Aug. 1973, pp. 337–344.

[8]Wellstead, P. E., "Reference Signals in Closed-Loop Identification," *International Journal of Control*, Vol. 26, 1977, pp. 945–962.

[9]Priestley, M. B., *Spectral Analysis and Time Series*, Vol. 1, Academic, London, 1981, pp. 528–563.

[10]Whitfield, A. H., "Transfer Function Synthesis Using Frequency Response Data," *International Journal of Control*, Vol. 43, May 1986, pp. 1413–1426.

[11]Sanathanan, S. K., and Koerner, J., "Transfer Function Synthesis as a Ratio of Two Complex Polynomials," *IEEE Transactions on Automatic Control*, Vol. 8, Jan. 1963, pp. 56–58.

[12]Young, P., and Patton, R. J., "Frequency Domain Techniques Applied to the Identification of Helicopter Dynamics," Control '88 IEE CP 285, April 1988, pp. 153–158.

[13]Whitfield, A. H., "Asymptotic Behaviour of Transfer Function Synthesis Methods," *International Journal of Control*, Vol. 45, March 1987, pp. 1083–1092.

[14]Marquardt, D. W., "An Algorithm for the Least-Squares Estimation of Nonlinear Parameters," *Journal of the Society for the Industrial Applications of Mathematics*, Vol. 11, June 1963, pp. 431–441.

[15]Bevington, P. R., *Data Reduction and Error Analysis for the Physical Sciences*, McGraw-Hill, New York, 1969, pp. 204–246.

[16]Hendricks, E., "Extended Kalman Filtering Applied to Helicopter Control," MSc Thesis, IMSOR, Technical University of Denmark, Lyngby, Denmark, 1980.

[17]Bramwell, A. R. S., *Helicopter Dynamics*, Edward Arnold, London, 1976.

[18]Mudge, S. K., and Patton, R. J., "Analysis of the Technique of Robust Eigenstructure Assignment with Application to Aircraft Control," *IEE Proceedings*, Pt. D, Vol. 135, July–Aug. 1988, pp. 275–281.

[19]Souza, E., Evans, R., and Goodwin, G. C., "Non-Linear Estimation Algorithms for Flight Path Reconstruction," TR EE8316, Univ. of Newcastle, Australia, 1983.

[20]Gelb, A. (ed.), *Applied Optimal Estimation*, MIT Press, Cambridge, MA, 1974, pp. 351–356.